

Observations and modelling of a clumpy galaxy at $z = 1.6$ ^{*}

Spectroscopic clues to the origin and evolution of chain galaxies

F. Bournaud¹, E. Daddi¹, B. G. Elmegreen², D. M. Elmegreen³, N. Nesvadba⁴,
E. Vanzella⁶, P. Di Matteo^{4,5}, L. Le Tiran⁴, M. Lehnert⁴, D. Elbaz¹

¹ Laboratoire AIM, CEA-Saclay DSM/IRFU/SAP – CNRS – Université Paris Diderot, 91191 Gif-sur-Yvette, France

² IBM Research Division, T.J. Watson Research Center, P.O. Box 218, Yorktown Heights, NY 10598, USA

³ Vassar College, Dept. of Physics & Astronomy, Box 745, Poughkeepsie, NY 12604, USA

⁴ Observatoire de Paris, GEPI, F-92195 Meudon, France

⁵ Observatoire de Paris, LERMA, F-75014 Paris, France

⁶ INAF – Osservatorio Astronomico di Trieste, Via G.B. Tiepolo 11, 40131 Trieste, Italy

Received; accepted

ABSTRACT

We investigate the properties of a clump-cluster galaxy at redshift 1.57. The morphology of this galaxy is dominated by eight star-forming clumps in optical observations, and has photometric properties typical of most clump-cluster and chain galaxies. Its complex asymmetrical morphology has led to the suggestion that this system is a group merger of several initially separate proto-galaxies. We performed H α integral field spectroscopy of this system using SINFONI on VLT UT4. These observations reveal a large-scale velocity gradient throughout the system, but with large local kinematic disturbances. Using a numerical model of gas-rich disk fragmentation, we find that clump interactions and migration can account for the observed disturbed rotation. On the other hand, the global rotation would not be expected for a multiply merging system. We further find that this system follows the stellar mass vs. metallicity, star formation rate and size relations expected for a disk at this redshift, and exhibits a disk-like radial metallicity gradient, so that the scenario of internal disk fragmentation is the most likely one. A red and metallic central concentration appears to be a bulge in this proto-spiral clumpy galaxy. A chain galaxy at redshift 2.07 in the same field also shows disk-like rotation. Such systems are likely progenitors of the present-day bright spiral galaxies, forming their exponential disks through clump migration and disruption and fueling their bulges. Our present results show that disturbed morphologies and kinematics are not necessarily signs of galaxy mergers and interactions, and can instead result from the internal evolution of primordial disks.

Key words. Galaxies: formation – Galaxies: kinematics and dynamics – Galaxies: high-redshift – Galaxies: evolution – Galaxies: interaction

1. Introduction

Giant molecular clouds and star formation complexes in present-day spiral galaxies have masses that rarely exceed 10^{-3} of the disk mass, and the total mass in these low-mass star forming regions does not dominate the disk mass. At high redshift ($z \simeq 1$ and above) the clumpiness and asymmetry of galaxies increases (Conselice 2003; Conselice et al. 2004; Daddi et al. 2004), which affects both the light fraction that is in the clumps and the individual masses of these clumps. Clumps at high redshift can be kpc-wide and as massive as $10^9 M_{\odot}$ (Elmegreen 2007, and references therein). In particular, the so-called "chain galaxies" have striking morphologies dominated by alignments of massive clumps (Cowie et al. 1996; van den Bergh et al. 1996; Moustakas et al. 2004). Dalcanton & Shectman (1996) first proposed that these chain galaxies could be edge-on low

surface brightness galaxy (LSB) progenitors at high redshift, but their clumps are one order of magnitude brighter than the star-forming regions of LSBs (Smith et al. 2001) and the clumps are not only bright star-forming complexes but are massive structures also visible in the near infrared (Elmegreen & Elmegreen 2005, hereafter EE05, see also NICMOS observations by Dickinson 2000). "Clump cluster" galaxies have the appearance of highly clumpy disks. Some are bulgeless, others have small red central concentrations that resemble primordial bulges. Because the photometrical properties of their clumps are similar to that of chain galaxies, Elmegreen et al. (2004) suggested that chains are the edge-on counterpart of such clumpy systems, which solves the problem of the face-on counterpart of chains being missing (O'Neil et al. 2000). The fraction of chains and clump clusters increases with redshift, and because these galaxies do not have an exponential profile already established, Elmegreen et al. (2005) proposed that they could be the progenitor of $z \sim 1$ spirals that further evolved into present-day bright spirals. They would thus be a crucial step in the formation of massive disk galaxies.

Send offprint requests to: F. Bournaud e-mail: frederic.bournaud@cea.fr

^{*} Based on observations obtained at the Very Large Telescope (VLT) of the European Southern Observatory, Paranal, Chile (ESO program ID 278.A-5009)

The origin of the massive clumps in chains and clump cluster galaxies, however, remains uncertain and largely debated. Noguchi (1999) and Immeli et al. (2004a,b) proposed that these could be dense fragments resulting from Jeans instabilities in gas-rich and bulgeless disks. Bournaud, Elmegreen, & Elmegreen (2007, hereafter BEE07) further explored this hypothesis and confirmed that these would evolve into spiral disks with a central bulge and an exponential disk (generally truncated in the form of type II as defined in Pohlen et al. (2007)). This hypothesis of internal instability however lacks clear support from observations so far. Spectroscopic observations of high-redshift disks unveil high turbulent speeds (Genzel et al. 2006; Förster Schreiber et al. 2006) so that the Jeans mass should be high and massive clumps could be formed, but these extensive spectroscopic surveys lack associated deep imaging to directly address the origin of clumpy galaxies. In contrast, Taniguchi & Shioya (2001) favored a multiple-merger origin involving several initially independent protogalaxies. In that vein, clump-clusters could be the high redshift equivalent of local compact groups, and some indeed have Stefan’s Quintet-like morphology (at the resolution of high-redshift observations). The merging subunits could be aligned along filamentary structures in the case of chains (Taniguchi & Shioya 2001). Even binary major mergers can look clumpy with several star forming knots (Goldader et al. 2002), and even an exponential profile would not exclude a merger origin (Moran et al. 1999). Complex morphologies with severe disturbances and asymmetries, like for instance bent chains or shrimp-like systems (Elmegreen & Elmegreen 2006; Elmegreen et al. 2007a) further suggest that an interaction/merger origin is plausible at least for these categories.

In this paper, we present kinematical IFU observations of the prototype clump-cluster galaxy UDF 6462 in the Hubble Ultra Deep Field (UDF). The morphology and photometry of this system at $z = 1.57$ have been studied in EE05 and Elmegreen et al. (2007b). A color image and an HST/ACS V-band image from the Hubble Ultra Deep Field (UDF, Beckwith et al. 2003) are presented in Fig. 1 and 2, the main photometrical properties are recalled in Sect. 2.1. This system is one that a priori poses a problem for the hypothesis of clumps being internally formed by instabilities in a massive disk: it is globally asymmetrical and has a Southern extension that resembles a spiral arm. Furthermore, two nearby systems (in projection) could be involved in an on-going interaction. UDF 6462 is classified as an on-going merger by Conselice et al. (2007).

Integral field spectroscopy data obtained with SINFONI on UT4 at ESO/VLT reveal complex internal kinematics, which has local disturbances but is overall dominated by a velocity gradient resembling that expected for an internally rotating system. Using the numerical simulations presented in BEE07, we propose a model of an unstable lopsided disk which forms internal clumps and, under some projections, a morphology resembling that of UDF 6462. We show that the observed velocity gradient and kinematical disturbances correspond precisely to those expected in such a scenario. Thus, this object that could a priori be regarded as being an on-going merger prototype, actually has properties that are fully compatible with the internally unstable disk hypothesis. Furthermore, the kinematics and some other properties are more difficult to explain in a multiple-merger scenario. Kinematical results of another nearby clumpy galaxy with

a bent-chain morphology (UDF 6911) at $z \simeq 2$ are also presented, and also show a large-scale velocity gradient favouring an internal disk fragmentation rather than a merger origin.

SINFONI observations of UDF 6462 are presented in Section 2. In Section 3, we present the numerical model that helps to interpret the morphological and kinematical properties of this system. In Section 4, we discuss the origin and evolution of this clump cluster galaxy, and our conclusions are summarized in Section 5. Spatially resolved SEDs in this system are presented in Appendix A ; numerical models of metals distribution in disks and mergers are discussed in Appendix B. In this paper we use a Chabrier (2003) IMF and standard cosmological parameters with $H_0 = 75 \text{ km s}^{-1} \text{ Mpc}^{-1}$. Throughout the paper, we will call *clumps* the large and dense structures typical of high-redshift clump-cluster galaxies, that have masses of $10^{8-9} M_\odot$ and typical sizes of the order of a kpc, much more massive than kpc-sized star-forming “clumps” of low-redshift spiral galaxies.

2. Observations

2.1. The UDF 6462 clump cluster

UDF 6462 (Fig. 1) has been imaged in B , V , i and z bands using HST/ACS and J and H bands with NICMOS. The main properties are summarised in Table 1. A spectroscopic redshift of $z = 1.570$ has been measured during the FORS2 campaign on the GOOD-S field (Vanzella et al. 2006, 2008) based on detection of the [OII] line. $BVIz$ data from Giavalisco et al. (2004) are presented and analyzed by EE05 and a photometrical analysis including NIR bands is in Appendix A. We here show V- and H-band images in Fig. 2 to recall the morphology of the system. EE05 estimate a stellar mass of $3.3 \times 10^{10} M_\odot$ and have identified 8 star-forming clumps in this system, with 36% of the total i_{775} luminosity in these clumps and 64% in a diffuse and redder inter-clump medium. The typical age of the clumps derived from optical photometry is around 310 Myr, while the inter-clump medium has a typical stellar age of nearly 3 Gyr. These properties, as well as the color-magnitude properties of the clumps, are globally typical of the sample of ten clump-cluster galaxies studied by EE05. The clump-cluster also has a central reddish blob, and the NIR emission is much more concentrated than the optical emission; this resembles a primordial bulge. In the following we will call this structure “*bulge*” and subsequently in the paper we will make the case for this; for the moment we only imply this word to be indicative of a location within the system and not presuming of its real nature.

The $B - i$ ACS image in Fig. 3 shows a color gradient from this red central proto-bulge to the bluer clumps. This is not simply reddening caused by higher extinction, considering that the region with red $B - i$ colors corresponds to the area of highest H-band surface brightness (see also SED fits in Appendix A). Photometric measurements compared with stellar population models suggest a bulge mass fraction of about 15–20%. This is actually an upper limit because of the NICMOS H-band resolution being larger than the red blob diameter. Spectral energy distributions of this central bulge-like blob and the other clumps are shown in Appendix A and also discussed in Section 4.

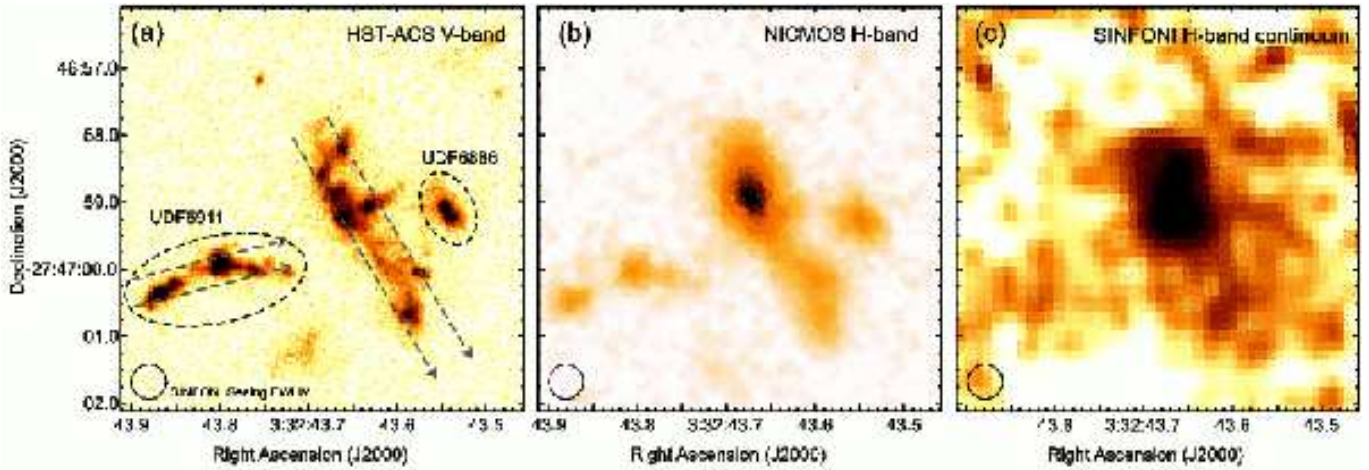


Fig. 2. The UDF 6462 clump-cluster: (a) HST-ACS V-band image plotted in log-scale. UDF 6911 and 6886 are very different redshifts (see text) and not interacting with UDF 6462. Dashed arrows indicate the pseudo-slits used to derive position-velocity diagrams. (b) NICMOS H-band image plotted in log-scale, showing a more concentrated emission around the central bulge-like blob. (c) H-band continuum from our SINFONI observations plotted in log-scale: UDF 6462 is detected, including its faint southern extensions; UDF 6911 is also detected.

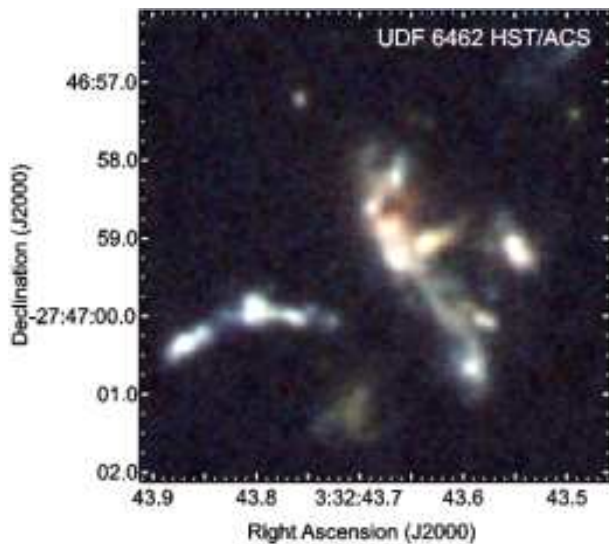


Fig. 1. Color image of the UDF 6462 clump-cluster from optical multi-band ACS imaging. The bent-chain UDF 6911 is visible to the left.

UDF 6462 has two neighboring systems, which we here denote UDF 6911 and UDF 6886 (see labelling in Fig. 2). UDF 6911 has a chain-like morphology, while UDF 6886 is more compact. The colors and dimensions are comparable to that of UDF 6462, possibly suggesting a similar redshift. We actually find from our SINFONI observations (see below) that these are at different redshifts.

The star formation rate (SFR) derived from the Spitzer MIPS $24 \mu\text{m}$ flux (Chary et al. in preparation) is $85 M_{\odot} \text{ yr}^{-1}$ based on the Chary & Elbaz (2001) models. This value could be an over-estimate because the $24 \mu\text{m}$ flux is likely contaminated by nearby systems. The UV-based estimate corrected for extinction is $50 M_{\odot} \text{ yr}^{-1}$, as in Daddi et al. (2007), and is not contaminated by nearby systems. The [OII] flux, corrected for extinction, corresponds to an SFR of $35\text{--}55 M_{\odot} \text{ yr}^{-1}$ (using relations

UDF 6462	
α (J2000)	$3^{\text{h}} 32^{\text{m}} 43.65^{\text{s}}$
δ (J2000)	$-27^{\circ} 46' 59.2''$
redshift	1.571
B mag	24.16
i mag	23.60
M_{\star}	$3.3 \times 10^{10} M_{\odot}$
SFR_{UV}	$50 M_{\odot} \text{ yr}^{-1}$
SFR_{IR}	$85 M_{\odot} \text{ yr}^{-1}$
$12 + \log(\text{O}/\text{H})$	8.53 ± 0.02
V_{circ}	$\sim 100 \text{ km s}^{-1}$

Table 1. Main properties of UDF 6462. Details and references are in Section 2.1.

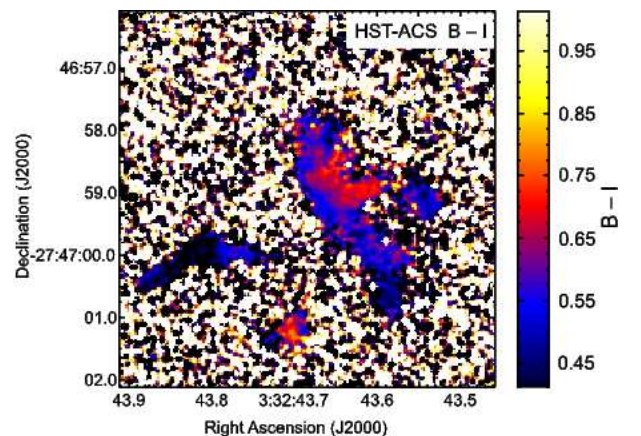


Fig. 3. $B - i$ color map of UDF 6462 from HST/ACS data, showing the color gradient from the central proto-bulge to the outer clumpy regions.

from Kennicutt 1998a). As the $24 \mu\text{m}$ flux may be contaminated by nearby systems (in particular UDF 6911 and 6886), these various estimates are consistent and suggest an SFR of about $50 M_{\odot} \text{ yr}^{-1}$ with an uncertainty around $20 M_{\odot} \text{ yr}^{-1}$.

2.2. SINFONI observations and data reduction

The observations were carried out using the SINFONI near-infrared integral field spectrometer mounted on the VLT UT4 telescope (Eisenhauer et al. 2003; Bonnet et al. 2004; Gillessen et al. 2005). An integration time of 5 hours was spent on the target in December 2006 with average seeing of 0.5 to 0.6'' in the H-band. No adaptive optics was used because no suitable Natural Guide Star was found close enough to the target. We used the high-resolution H-band grism, which offers a FWHM spectral resolution of $R \simeq 3000$ in the H-band, equivalent to a FWHM of $\sim 90 \text{ km s}^{-1}$ for the $\text{H}\alpha$ line at $z = 1.57$. A first standard reduction of the data has been performed using the SINFONI pipeline (Modigliani et al. 2007).

We then performed a more careful reduction relying on a set of standard IRAF tools to reduce longslit spectra (Tody 1993), which we modified and extended by a set of IDL routines matched to the special requirements of SINFONI. The dark-frame subtracted and flat-fielded data are rectified using an arc lamp (for the spectral direction) and an artificial point source (for the spatial direction). To account for some spectral flexure between frames, we rectify the data before sky subtraction. We correct for variations of the sky background in the object and the sky frame by rescaling the count rate of the sky frame to that of the corresponding object frame, carefully masking the object, before reconstructing, aligning, and combining the three-dimensional data cubes. Flux scales are obtained from standard star observations taken once per hour at an air mass and position which match those of the source. We also used stars to measure the spatial resolution. The spectral resolution was measured from night sky lines. For a more detailed description see, e.g., Nesvadba et al. (2006). The data presented hereafter are those obtained with this careful reduction, but we checked that all features discussed in the paper are also seen in the dataset reduced with the standard SINFONI pipeline procedure.

2.3. Spectroscopic redshift and neighbouring systems

We identified the $\text{H}\alpha$, [NII] and [SII] emission lines associated with UDF 6462 in the SINFONI datacube; the associated spectroscopic redshift is $z = 1.571$. In UDF 6911, we detect the [OIII] and $\text{H}\beta$ emission; the associated redshift is $z = 2.071$. As for UDF 6886, a single emission line is detected and assumed to be the $\text{H}\alpha$ line; in this case the redshift is $z = 1.427$. Results on the internal kinematics of UDF 6911 are shown in Section 4.3. The emission line of UDF 6886 is not spatially resolved in our data.

The integrated spectrum of UDF 6462 is shown in Fig. 4. The HII emission line from UDF 6462 falls far enough from telluric OH lines so that robust moment maps can be extracted. The detection of [NII] and [SII] emission is fainter and limited to the central regions. Because these lines are faint and/or contaminated by OH lines, associated velocity fields could not be properly retrieved over a significantly extended area.

The H-band continuum map of the system is shown in the third panel of Fig. 2. This continuum map is based only of the parts of the spectrum that are not affected by an OH sky line or another emission line. Linear interpolations were used to recover the continuum over the regions affected by

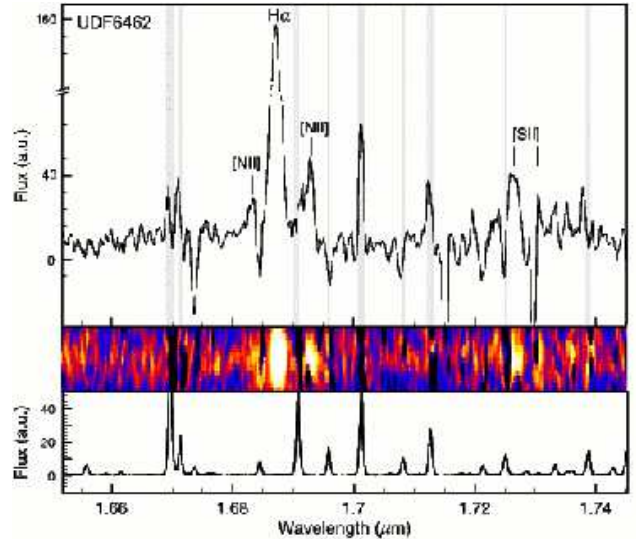


Fig. 4. Integrated spectrum of UDF 6462 central regions (top). Sky lines are shown below. Shaded bands corresponds to wavelength ranges where the sky emission level exceeds the average $1\text{-}\sigma$ noise level estimated on the continuum. The HII line from UDF 6462 falls in a region free of telluric OH lines for at least $\pm 600 \text{ km s}^{-1}$ around the central wavelength. The [NII] $_{\lambda 6582}$ line is also unaffected by sky lines. The 2-D spectrum shown on the middle corresponds to a pseudo-slit ranging from $\delta = -27^\circ 47' 58.5''$ (top) to $\delta = -27^\circ 47' 59.5''$ (bottom); the pixel size on this plot is the raw SINFONI pixel size in both the spatial and spectral directions.

these lines, and the continuum intensity was finally computed for wavelengths within the H-band range.

The two companions of the main system have largely different redshifts. In spite of their apparent proximity, similar colors and comparable clump sizes, these are not nearby systems in the 3-D Universe. The spurious apparent proximity and similarity of these systems illustrates that the identification of interacting/merging galaxies at high redshift without accurate spectroscopic redshifts cannot be rigorous. In the present case, the disturbed morphology of UDF 6462 could have further suggested an on-going interaction with its apparent companions, which spectroscopic redshifts rule out, showing that morphology is not always a good tracer of on-going galaxy interactions.

UDF 6462 is *not* interacting with its apparent neighbors; nevertheless this does not rule out a merger origin for this system itself. The blobs gathered into this irregular clump cluster may still be several independent units merging together instead of internal fragment of a single system, and this is what is studied in the following.

2.4. Results: kinematics of the UDF 6462 clump cluster

The first moment map associated with the $\text{H}\alpha$ emission line in UDF 6462 is shown together with the $\text{H}\alpha$ intensity contours in Fig. 5. The main regions are detected with a signal-to-noise¹ (S/N) ratio above 3. The detection of the Southern blob is more uncertain, at about $\text{S/N}=2.6$, but this blob is also seen on the Position-Velocity (P-V) dia-

¹ we measured the S/N ratio as the ratio of the flux in the HII line to the noise measured on the continuum, following for instance Flores et al. (2006) with a single line in our case.

gram shown in Fig. 6, on the continuum map (Fig. 2). The velocity field in the main region shows a large-scale velocity gradient with the Northern parts approaching and the Southern parts receding. The (suspected) Southern blob follows the same trend. One can however note that this velocity gradient is severely disturbed compared to what would be expected for a usual rotating disk. The V/σ ratio² is typically between 1 and 2. In particular, Fig. 5 shows several clumps with velocities larger or smaller than expected for a purely rotating system. The P-V diagram along the apparent major axis of UDF 6462, shown in Fig. 6, confirms the overall trend for a velocity gradient throughout the system but with local disturbances; in particular a clump at $\delta = -27^\circ 47' 59.4''$ in the observation on Fig 6 has a velocity lower than expected from the large-scale gradient, and a similar perturbation is found in the model at $X=4$ kpc in the same figure.

The kinematics of UDF 6462 thus shows some sign of rotation, with on average a velocity gradient along the major axis of the system. The velocity dispersion map shown in Fig. 6 has a maximum in the dispersion around $\delta \simeq -27^\circ 46' 58.8''$ which is the region where the velocity gradient on the P-V diagram is maximal. This is a signature expected for rotation (e.g., Förster Schreiber et al. 2006; Genzel et al. 2006; Puech et al. 2006), in particular because the high-dispersion region is extended in the direction perpendicular to the velocity gradient (i.e., along the morphological minor axis). Moreover, the highest slope in the P-V diagram lies on the continuum peak, which further indicates that this velocity gradient traces a rotation curve rather than some other kind of motion.

This underlying large-scale rotation pattern is, however, largely disturbed at the local scale of individual clumps. Some have velocities smaller or larger than expected for pure rotation, with discrepancies up to $40\text{--}50 \text{ km s}^{-1}$. This is larger than the velocity anomalies caused by spiral arms and other internal structures in classical low-redshift disk galaxies (e.g., Rots 1975). As a result, the velocity dispersions and local kinematical disturbances are high, nearly comparable to the rotation velocity if the large-scale gradient is tracing rotation.

2.5. Metallicity and central enrichment in UDF 6462

Intensity maps of the [NII] and [SII] emission lines are displayed in Fig. 7. The [NII] and [SII] emissions seem more centrally concentrated than the $H\alpha$ emission. Metallicity estimates, based on [NII]/ $H\alpha$, within an aperture centered on the surface brightness peak in the H-band compared to that of the entire system, suggest that this region of high metallicity is real and not due to lower signal to noise in the outer regions of emission.

We used the N2 ratio, defined by $N2 = \log([NII]_{\lambda 6584}/H\alpha)$, as a proxy for the Oxygen abundance, as proposed by Storchi-Bergmann et al. (1994). Pettini & Pagel (2004) determined the relation:

$$12 + \log(O/H) = 8.90 + 0.57 \times N2 \quad (1)$$

The N2 ratio in UDF 6462 supports star formation as the powering source of the optical lines (Erb et al. 2006a;

Halliday et al. 2008), consistent with the fact that this system does not show a mid-infrared excess typical of AGNs. The N2 ratio is also not as high as it could be for systems with strong winds (Lehnert & Heckman 1996). To derive the bulge metallicity, we measured intensities inside a $0.6''$ diameter aperture centered on the NICMOS H-band emission peak. The global metallicity was derived inside the $3\text{-}\sigma$ contour of the $H\alpha$ flux map. We find:

- $12 + \log(O/H) = 8.59 \pm 0.04$ for the bulge
- $12 + \log(O/H) = 8.53 \pm 0.02$ for the whole system

where the indicated uncertainties correspond to the estimated noise level in emission maps³. This corresponds to a metallicity of $Z \simeq 0.5Z_{\odot}$ for the whole system. The calibration of the N2 ratio might suffer from systematic uncertainties, but there is rather robust evidence for central enrichment in this clump-cluster system. The relative Oxygen abundance in the central redder blob is about 20% higher than in the rest of the system. The whole system agrees with the mass-metallicity relation of $z \sim 2$ established by Erb et al. (2006a) and Halliday et al. (2008) and has a slightly lower metallicity than Luminous Infrared Galaxies at $z \simeq 0.6$ (Liang et al. 2004), but the bulge metallicity alone is significantly enriched and would be in between the $z \sim 2$ relation and that of low redshift galaxies (SDSS, Tremonti et al. 2004). The metallicity map obtained from the N2 ratio displayed in Fig. 7 shows this central enrichment, and a radial metallicity gradient spanning from the central red bulge towards the rest of the system.

3. Numerical Modelling

Large kinematical disturbances are frequently interpreted as evidences for interaction/mergers, in particular when they are associated with complex morphologies (see Introduction). In the following, we use an N -body numerical model to study whether an internal origin for the star-forming clumps in UDF 6462 could be another viable explanation of such properties.

3.1. Simulation technique

The numerical technique used here is similar to that presented in more detail in BEE07 and references therein; we here only recall the main aspects. The N -body code models stellar, gaseous, and dark matter particles. The gravitational potential is computed on a 256^3 grid using an algorithm based on Fast Fourier Transforms and optimized for vector computers. The grid cell size and gravitational softening length are 180 pc. We use 2×10^5 stellar particles, 2×10^5 gas particles, and 3×10^5 dark matter particles. Star formation is accounted for using a local Schmidt law with an exponent 1.5 (Kennicutt 1998b). This 1.5 exponent is applied to the gas volume density in our models, which is equivalent to applying it to the surface density assuming a constant thickness, as is the case in our initial conditions. The dissipative nature of the turbulent interstellar medium is modeled with a sticky-particle scheme.

² The V/σ ratio here is not corrected for inclination because the inclination is unknown (or model-dependent), so it is not a direct indicator of the rotational support in this system.

³ Because our data are not flux-calibrated, these error bars are only related to the spatial variations of O/H; a constant additional offset may affect both measurements in the same way.

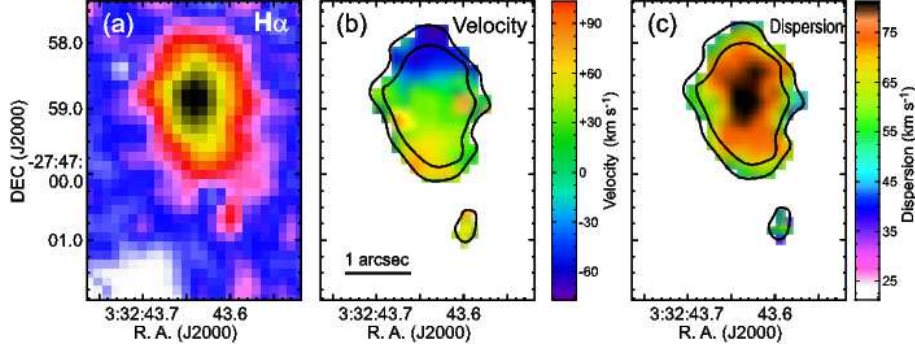


Fig. 5. Moment maps for the $H\alpha$ line from our VLT/SINFONI data. (a) $m = 0$ intensity map, (b) $m = 1$ velocity field, and (c) $m = 2$ velocity dispersion field for UDF 6462. The $2\text{-}\sigma$ and $5\text{-}\sigma$ contours of the zero moment map are shown; the southern blob is detected at about $2.6\text{-}\sigma$, with a continuum signal at the same location (Fig. 2). Instrumental broadening was subtracted from the dispersion map. UDF 6462 shows signs of rotation with a velocity gradient and a central peak in the velocity dispersion; however kinematical disturbances are larger than in classical low-redshift disk galaxies.

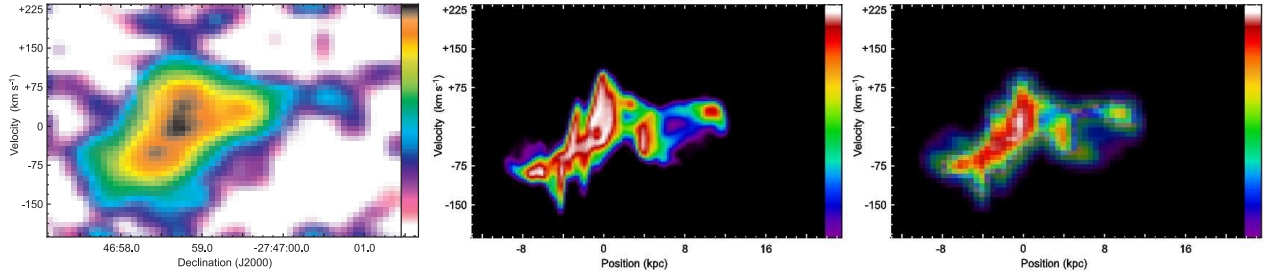


Fig. 6. **Left:** Position-Velocity diagram of UDF 6462 along its apparent major axis. The thick pseudo-slit used to compute this diagram is shown in Fig. 2, data have been resampled to a twice smaller pixel size on this P-V diagram. Note the global velocity gradient corresponding to the velocity field in Fig. 5, the steepest parts of the gradient around the emission peak corresponding to the peak in the line-of-sight velocity dispersions. **Right:** Position-Velocity diagram for the model in Section 3, along its projected major axis, at full resolution and degraded to the spatial seeing, pixel size and instrumental velocity resolution. A global velocity gradient as in UDF 6462 is reproduced, together with large local disturbances and rather high velocity dispersions. Each clump in this modeled clump-cluster has an internal velocity gradient associated with its own spin, which could not be resolved at the SINFONI resolution.

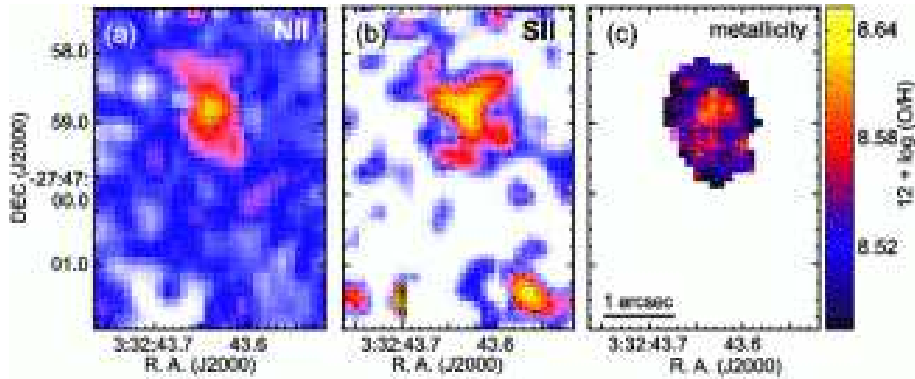


Fig. 7. (a,b) [NII] and [SII] intensity maps of UDF 6462. Metals appear to be centrally concentrated around the reddish proto-bulge and UDF 6462 shows sign of central enrichment illustrated by the metallicity map (c) where the O/H ratio is estimated from the [NII]/HII flux ratio (see text).

3.2. Model parameters

The physical parameters of the model presented here are close to that of model 6 in BEE07, except that a moderate initial asymmetry is introduced in the system. The baryonic disk initially has a flat radial profile (uniform surface density). This is because clump-cluster galaxies generally do not have a spiral-like exponential profile, but generally show irregular and less concentrated profiles (e.g., Elmegreen et al. 2005), which is the case for UDF 6462 at least in optical bands. The hypothesis of a uniform surface density was made because it is a simple and not restrictive choice already made in BEE07 models, but is not required to produce a clump-cluster morphology – clump interactions and migration will anyway rapidly redistribute the disk mass.

This disk has a radius of 8 kpc radius and a mass of $6 \times 10^{10} M_{\odot}$, with a constant scale-height of 700 pc. The initial gas fraction is 50%, giving a stellar mass of $3 \times 10^{10} M_{\odot}$. Stars are initially given random motions with a Toomre parameter $Q_s = 1.3$, and gas particles have a velocity dispersion of 11 km s^{-1} .

As the central blob of UDF 6462 is redder than the rest of the system and could be a primordial bulge, a spherical bulge of 14% of the disk mass is added to the initial conditions in the model. This bulge fraction is compatible with observational estimates for UDF 6462 (15-20% from the SED fits in Appendix A), because 14% is the initial fraction in the model, which grows with time during the clump cluster evolution, and because the observed value is

⁴ This is compatible with the observational estimate (see Sect. 2.1) once some more stars have formed in the simulation

an upper limit to the actual bulge mass. Note furthermore that the bulge mass is not a crucial parameter to study the large-scale kinematics of clump cluster formed from fragmented disks: even bulgeless models in BEE07 show the same kinematical properties (disturbed rotation) as we find below for the present model.

The dark matter halo is modeled as a Plummer sphere of total mass⁵ $2.9 \times 10^{11} M_{\odot}$ and scale-length 12 kpc, truncated at 24 kpc. The dark-to-visible mass ratio within the initial disk radius is 0.35. Models of unstable disk evolution with NFW dark matter profiles are presented in Elmegreen et al. (2008b), and the different halo profile does not radically change the evolution of clump clusters formed this way.

Because the observed system is asymmetrical, the disk center is spatially offset from the halo and bulge mass centers by 10% of this radius. Given that the degree of morphological lopsidedness in present-day spirals is frequently as large as 10 or even 20% (e.g., Bournaud et al. 2005; Angiras et al. 2007; Reichard et al. 2007) this is a realistic, moderate initial asymmetry⁶. The first snapshot in Fig. 8 illustrates the initial asymmetry.

3.3. Morphology

The gas-rich, unstable disk in the present model is similar to the one studied in BEE07 and follows a similar evolution. The disk fragments into massive clumps in about 10^8 years, the formation of which can be followed in Fig. 8 and 9. This system forms eight big clumps embedded into a fainter underlying disk; the mass fraction in the clumps reaches a peak value after $t = 270$ Myr when 41% of the disk mass is gathered in the clumps.

Because of the initial asymmetry, the clump distribution itself can appear quite asymmetric. Depending on the projections, the clumpiness can increase the apparent asymmetry. For instance, the last instant in Fig. 8 would have a high apparent asymmetry seen from the bottom-right, and a lower asymmetry seen from the bottom-left. We also note the development of an lopsided spiral structure from the initial asymmetry and instability. This structure resembles the Southern extension of UDF 6462, which might thus be formed without an external tidal interaction.

The instability of this massive gas-rich disk, combined with its moderate initial asymmetry, results in the quite asymmetrical and clumpy projection shown in Fig. 9 with an inclination of 64 degrees. This projection is morphologically similar to the HST V-band image of UDF 6462 shown in Fig. 2.

3.4. Kinematics

We show in Fig. 9 the velocity field of the modeled clump cluster for the projection which looks similar to UDF 6462. The velocity field shows a large-scale velocity gradient, but local variations and irregularities can be seen which resemble those observed in the SINFONI velocity field of

UDF 6462. In addition, the P-V diagram along the apparent major axis is shown in Fig. 6, both at full resolution and at the SINFONI resolution. Clumps on this P-V diagram show an internal spin that could not be detected at the SINFONI resolution. On larger scales, clumps follow a global velocity gradient associated with the rotation of the system, but the individual velocity of each clump can be offset from this global gradient by a few tens of km s^{-1} . Similar kinematical irregularities are also shown for some cases in BEE07, and are caused by clumps interacting together and migrating in the system. In the present case, the P-V diagram of the system also incorporates the asymmetry, which gives it an overall aspect qualitatively similar to the observed one shown in Fig. 6. A velocity gradient can be detected and traces the overall rotation of the system, but the internal evolution of the clump cluster causes significant disturbances to the kinematics, that are larger than the disturbances caused by spiral arms and internal structure in regular spiral disks (e.g., Rots 1975).

The observed peak-to-peak velocity extension of the P-V diagram of UDF 6462 is about 120 km s^{-1} . Assuming that the circular velocity is traced by the envelope at 50% of the peak level (e.g., Donley et al. 2006), the projected circular velocity $V_c \sin i \simeq 90 \text{ km s}^{-1}$. Assuming an inclination $i = 63$ deg, as suggested by our numerical model and consistent with the observed morphology, this corresponds to a circular velocity of about 100 km s^{-1} .

Both the morphological and kinematical properties of UDF 6462 are qualitatively reproduced by the clump-cluster model presented here, at the instant and under the projection that we have chosen. We do not claim that the real system has followed exactly the same evolution in particular, because we simply picked a similar-looking model among several ones, and the solution is probably not unique. Nevertheless, the present model illustrates the fact that the clumpy morphology and the disturbed kinematics of UDF 6462 can be reproduced by models based on the internal evolution of unstable gas-rich disks: this model shows that the morphology, clumpy and asymmetric, and the kinematics with local perturbations, can both be accounted for by the internal evolution of gas-rich disks. To achieve this, we have here added a moderate initial asymmetry in the present model, which under a chosen projection reproduces the peculiar morphology observed for this system and its disturbed morphology at the same time. Other models presented in BEE07 show similar morphologies and kinematical disturbances of the same order, even if not reproducing the individual case of UDF 6462.

4. Discussion

4.1. UDF 6462: Unstable disk or multiple merger?

The UDF 6462 clump cluster has been considered a good candidate for a merging system, because of its irregular and asymmetrical morphology compared to some other chain galaxies that have more symmetrical aspects. In such a group model, initially separate dark matter haloes with their stellar and gaseous content each would be merging together, and be presently observed in a phase resembling a compact group. It could also be a binary merger with several star forming clumps.

⁵ This total mass is that of the un-truncated sphere.

⁶ There are furthermore reasons to assume that $z \sim 1$ disks are more lopsided than $z \sim 0$. Be these asymmetries caused by interactions, by asymmetrical gas infall, or by halo asymmetries, these causes themselves should be more frequent/efficient at high redshift.

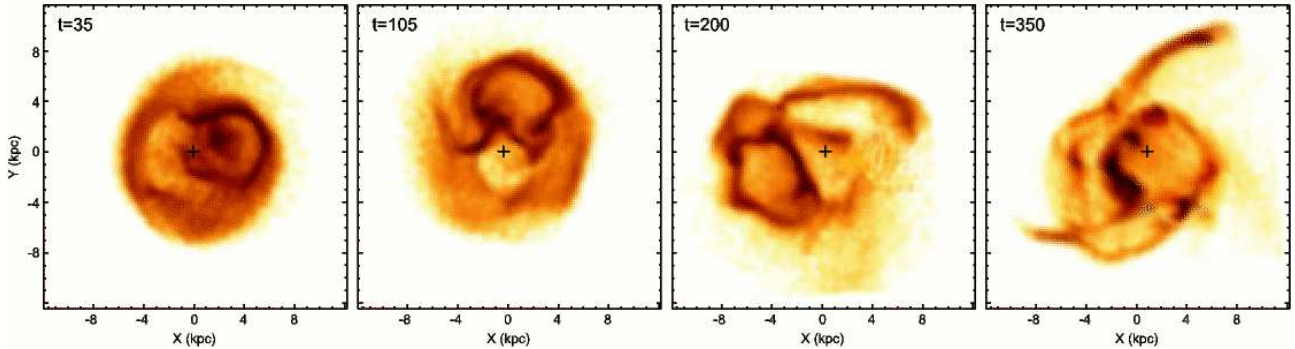


Fig. 8. Snapshots of the disk mass density in the model, with time indicated in Myr. The halo mass center is marked by the black + symbol. The initial conditions are closely similar to the first snapshot, with a uniform disk density. The last snapshot shown here is slightly before the projection reproducing the UDF 6462 morphology (Fig. 9). Note that the asymmetrical aspect resulting from the initial disk-halo offset is amplified by a long spiral arm extension and the outer location of one of the clumps.

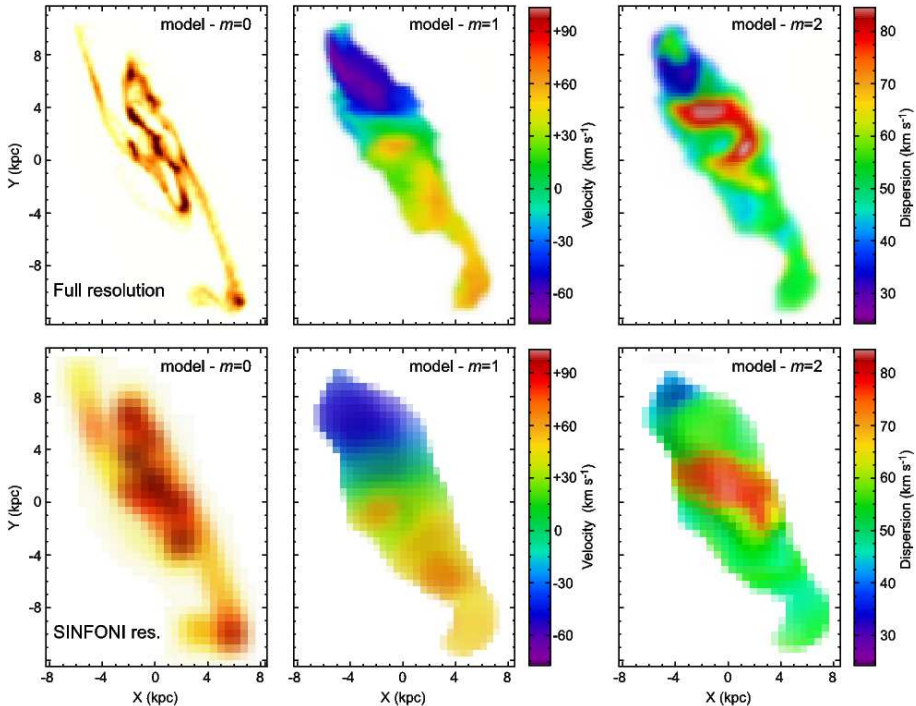


Fig. 9. Projection of the model reproducing the UDF 6462 clump-cluster morphology, after 380 Myrs of evolution. **(a)** projected density map of stars formed less than 300 Myrs ago to mimic the V-band map shown in Fig. 2. **(b)** line-of-sight velocity map. The velocity field was smoothed to a 1 kpc resolution (Gaussian smoothing) to reduce the numerical noise, and a cut-off along an isodensity contour was applied. **(c)** line-of-sight velocity dispersion map. Under this projection, model qualitatively reproduces the severely disturbed rotation pattern observed in UDF 6462, with a large-scale velocity gradient and a central peak in the velocity dispersion. **(d,e,f)** Same moment maps degraded to the spatial resolution of our SINFONI observations. Irregularities in the velocity field are still visible, for instance the high-velocity region around $X=-2$ and $Y=-1$ kpc, which is comparable to the velocity anomalies observed in UDF 6462.

However, our numerical model shows that such a complex morphology can result from the internal evolution of an unstable gas-rich disk galaxy. In this fragmentation model, a single dark matter halo contains or accretes large amounts of gas, so that the primordial disk can become Jeans-unstable and fragments into several large star-forming clumps, taking the appearance of a clump-cluster. Only a moderate (realistic) initial asymmetry is needed in the model to qualitatively reproduce the projected morphology of UDF 6462. The kinematic data obtained with SINFONI unveil a large-scale velocity gradient, together with local disturbances. Such a large-scale velocity gradient is a signature expected for a clump cluster formed by internal instabilities in a disk galaxy. The irregularities in the velocity field are then explained by clump-clump interactions that cause the individual velocity of each clump to differ significantly from the initial rotation velocity. Both the morphology and the kinematics of UDF 6462 can thus be accounted for by an unstable disk scenario.

The viability of this first scenario does not strictly rule out a merger origin. The blobs observed in UDF 6462 could be initially independent sub-units merging together at the same time to form a more massive galaxy. However, several observed properties appear unlikely under this hypothesis:

- (1) First, the clumps have comparable masses and sizes (see Figs. 2 and A.1) which is typical of most chains and clump cluster galaxies. The dynamical friction timescale for merging galaxies is inversely proportional to the mass. Blobs that have the same mass as the most massive one should merge rapidly, and low-mass blobs should survive longer. The present morphology of UDF 6462 could then only be a transient one, unlikely to be observed. A massive blob surrounded by several lower-mass ones would be a more likely configuration. On the other hand, the similar masses for all clumps are naturally expected for the internal fragmentation of a primordial disk, because the typical clump mass in this case would be the Jeans mass in the outer disk.

- (2) The large-scale rotation-like velocity gradient and the central peak in the velocity dispersion are also characteristics of rotating disks that are predicted to be preserved (with disturbances) in a clump cluster formed from an unstable disk. Such properties are not necessarily expected for a merging system. In particular, there is no reason for which merging blobs would be globally rotating in the same direction. The observed velocity dispersions are rather high but do not dominate the large-scale velocity gradient; for a multiple merging they would more likely be larger the rotation velocity. Actually the merging timescale is faster for systems that rotate in the same direction, because of angular momentum removal in tidal tails, while counter-rotating systems take longer to merge. The absence of counter-rotating unit among the several blobs is a possible but unlikely property for a multiple merger origin.
- (3) The radial metallicity gradient (Fig. 7) with central enrichment in the reddish bulge-like blob is also expected for a (clumpy) disk, and the total metallicity is about that expected for a disk of this mass. The centrally concentrated $[\text{NII}]/\text{H}\alpha$ ratio is similar to what Förster Schreiber et al. (2006) found in a rotating disk at $z \simeq 2$ (Q2343-BX610), with a ratio between the central metallicity peak and the outer disk metallicity larger by 35% but comparable to what we find here in UDF 6462. Such a disk-like metallicity distribution would be another coincidence if UDF 6462 is an-going group merger. Generic models of galaxy mergers and disk fragmentation in Appendix B confirm that a radial metallicity gradient is better preserved by the disk fragmentation mechanism than in early-stage galaxy mergers with clumpy morphologies.
- (4) Stellar population studies confirm that the clumps are young, star-forming objects around an older, central, bulge-like object. The observed SEDs and theoretical fits for the whole galaxy, the bulge, and several clumps are shown in the Appendix A and Fig. A.1. The central region that we have called bulge is clearly redder than the clumps. The reddest clump is an extended region jutting off from the bulge and may be part of the bulge. The central reddish bulge has an age around 1 Gyr. The clumps have an age of ~ 50 Myr with a comparable decay time in the star formation rate. There appears to be no significant old stellar component in the clumps other than the central bulge: if these clumps were separate galaxies in a merging process, they should have older stellar components in them, formed before this merger as in any galaxy. The absence of old stars in the clumps further supports our model in which they formed recently by the fragmentation of a gas-rich disk. Moreover, these clumps appear to have similar ages (similar SED slopes) which again arises naturally in the disk fragmentation scenario.

The observed properties of UDF 6462 are thus consistent with an unstable-disk origin, while they would be unlikely coincidences in a merger origin. We also note that a stellar mass of $3.3 \times 10^{10} M_{\odot}$ and an external diameter of ~ 10 kpc (without the low-mass Southern extension) would place the system in agreement with the mass-size relation of disk galaxies from Trujillo et al. (2006) which, at a slightly higher redshift of 1.7, indicates an *half-light* diameter of 6 kpc for a galaxy of this mass. Furthermore, the

5 kpc radius and 100 km s^{-1} circular velocity inferred above are consistent with the size-velocity relation observed for star-forming disks at $z=1.5-2$ by Bouché et al. (2007), while submillimeter galaxies (likely major mergers) are found to have much lower size:velocity ratios by these authors.

These various properties cannot definitely rule out a merger origin, also because only one system with direct evidence for massive clumps from HST/ACS and NICMOS imaging has been studied so far. However, for the merging of a group of initially separate galaxies, one would expect a concentration of dark matter around each visible blob, so that the largest velocity gradients should be internal to the clumps, and not in the form of a global rotation of the system. One might assume that, in a merger model, the initially separate dark haloes could have merged into a single one, while their baryonic counterparts would still be separate. However such a system should resemble Local Compact Groups, in which the prominent kinematical signatures are internal gradients inside each galaxy with little global rotation of the group (e.g., Amram et al. 2007, and references therein). Local systems have lower gas fractions, but tidal interactions in the early stages of mergers are dominated by the DM and stellar potential, so that the kinematic response of the gas would at first order be similar in higher redshift compact groups. This comparison further confirms that the properties of UDF 6462 are unlikely for a merger mechanism. On the other hand, the fragmentation model within a single dark matter halo predicts (see the simulation here and those in BEE07) that clumps have some internal rotation, but with low velocities (a few tens of km s^{-1}), which could not be detected at the SINFONI resolution (see Fig. 6). The velocity dispersions are rather high for a disk (compared to regular spirals), with $V/\sigma \simeq 1.5-2$ in the observations and $V/\sigma \simeq 2.5$ in the model. The small difference is likely explained by the larger beam size in observations. Models of galaxy mergers usually result in much lower V/σ ratios, smaller than 0.5 in the case of multiple mergers (e.g., Bournaud et al. 2007).

UDF 6462 is presently a quiescent galaxy. Its star formation rate to stellar mass ratio $SFR/M_{\star} \simeq 1.5 \text{ Gyr}^{-1}$, which is consistent with the typical $SFR - M_{\star}$ relation found for galaxies of this mass by Daddi et al. (2007) at $z \sim 2$. Stellar population studies in EE05 however suggest that the star formation activity was somewhat stronger in the last few 10^8 yr. The formation of massive clumps in gas-rich disks can indeed trigger star formation: models in BEE07 typically reach star formation rates of $30-40 M_{\odot} \text{ yr}^{-1}$, up to ten times higher than the progenitor axisymmetric disks. Immeli (2004a) reports even higher star formation rates of $200 M_{\odot} \text{ yr}^{-1}$ but in the more extreme case of initially gas pure disks nearly as massive as the Milky Way. The lifetime of these systems in BEE07 is about $0.5-1$ Gyr, which is actually a lower limit because regulation by supernovae feedback was not included in these models. The circular velocity and dispersion estimated above corresponds to a dynamical (total) mass of $\sim 4 - 5 \times 10^{10} M_{\odot}$ within the optical extent of the system, consistent with the stellar mass (Section 2.1) and implying a rather moderate ($\sim 20\%$) gas fraction at the observed instant⁷. However, an SFR of $\sim 50 M_{\odot} \text{ yr}^{-1}$ and an age of $\sim 3 - 4 \times 10^8$ yr imply an

⁷ assuming that the mass within the optical radius is mostly visible with little contribution from the halo, as is generally the case for Local disk galaxies

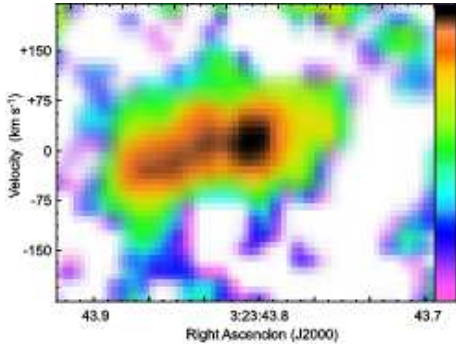


Fig. 10. Position-Velocity diagram of UDF 6911 along its apparent major axis, in the [OIII] emission line. The thick pseudo-slit used to compute this diagram is shown in Fig. 2.

initial gas fraction of about 50%, so that these mass estimates are compatible with the starting conditions of our model. We also note that this 50% initial gas fraction in the model is in agreement with observations by Erb et al. (2006b) and Daddi et al. (2008) and assumptions in Bouché et al. (2007). Furthermore, models with different initial gas fraction in BEE07 also show disturbed rotation comparable to the present case.

Although the present models are initially asymmetric and highly complex structures develop quickly, real galaxies could be even more complex, especially in the off-plane dimension, as a result of active inflow from cosmic streams and previous mergers. However, the model clearly indicates how internal clumpiness in a gas-rich galaxy can affect the kinematics. The comparison with observed properties then shows that the scenario in which the UDF 6462 clump cluster would have formed by internal instabilities in a gas-rich disk is a fully plausible one, in spite of the complex morphology and disturbed kinematics. These observed properties can be explained, and the global rotating expected in this scenario is observed as a large-scale velocity gradient throughout the clump cluster.

4.2. Kinematics of the bent-chain UDF 6911

The Eastern companion of UDF 6462, UDF 6911 (Fig. 2), has the elongated morphology of a bent chain galaxy at $z = 2.07$. The same question on its origin can be posed as for UDF 6462. The kinematics of this system is only poorly resolved in our SINFONI data. The P-V diagram of the [OIII] emission line along the apparent major axis of this object is shown in Fig. 10. Here again, we detect a velocity gradient with a shape compatible with the flat rotation curve expected for a disk galaxy. Assuming that the circular velocity is traced by the envelope at 50% of the peak level (e.g., Donley et al. 2006) to account for beam-smearing effects, and that this system is observed close to edge-on, the rotation velocity is estimated to be about 75 km s^{-1} . The resolution is too low to unveil local disturbances, but at least the global rotation pattern expected for a fragmented disk is found here, indicating that this interpretation is fully possible for this second object as well as for UDF 6462.

4.3. Clump clusters and spiral disk and culge progenitors, and their role in the star formation history

Within the plausible scenario where UDF 6462 and UDF 6911 (and possibly other clump clusters and chain galaxies) formed by internal fragmentation of clumpy disks, primordial galactic disks have to accrete enough mass at high redshift so that large fragments of their disks can collapse through gravitational instabilities. The presence of large gas reservoirs around disk galaxies at $z \sim 1.5$, unveiled recently by Daddi et al. (2008), shows that large amounts of gas representing at least half of the total baryonic mass can indeed be accumulated around primordial galactic disks. Massive disks with such high gas fractions are then likely to be gravitationally unstable and fragment into clump-cluster galaxies, or chain galaxies when seen edge-on, clump-clusters being face-on counterparts of the later as already suggested by Elmegreen et al. (2004).

Fragmentation of gas-rich disks into clump clusters can then be an efficient mechanism to trigger star formation, with an efficiency at least comparable to that of major merger, if not higher, and longer star-formation timescales. Indeed, numerical models of merger-induced starbursts indicate that, on average, these have only modest intensities and durations (Di Matteo et al. 2007) even if some particular cases can be very efficient (e.g., Cox et al. 2006). Recent observations further suggest that galaxy interactions and mergers have a modest influence on the cosmic star formation history (Jogee et al. 2008) and that internal processes in gas-rich disks play a more important role (Daddi et al. 2008). In a sample of Luminous Infrared Galaxies at $0.4 < z < 1.2$, Zheng et al. (2004) have identified a majority of disk and irregular galaxies and a relatively small fraction of mergers.

Later on, the clumps migrate towards the central region, being also progressively disrupted by the tidal field and their mutual interactions and redistributing the underlying disk mass into an exponential disk, as shown by numerical simulations (Carollo et al. 2007, BEE07). Bulges with masses up to $\sim 30\%$ of the baryonic mass can be formed, or grown if already present, by the central merging of clump remnants; the bulges formed this way have the properties of the classical bulges of spiral galaxies (Elmegreen et al. 2008b). Associated central black holes can be accreted at the same time from intermediate mass black holes formed by stellar collisions in the core of clumps, possibly explaining the black-hole-bulge scaling relations without mergers (see Johansson et al. 2008, for the case of mergers). Clump cluster and chain galaxies, when formed by the fragmentation of gas-rich primordial disks, are thus possible progenitors of present-day bright disk galaxies, as already suggested by van den Bergh et al. (1996).

Clump clusters were found by BEE07 to form a thick disk of old stars, together with a thinner disk of gas and younger stars, which can further grow in mass by continued accretion. One can notice that the rotation velocity found in UDF 6462 is lower than what would be expected for the stellar mass from the Tully-Fisher relation (Conselice et al. 2005). As the thick disks of spiral galaxies are observed to have a lack of rotation compared to thin disks (Yoachim & Dalcanton 2005, 2006), clumpy evolution at high redshift is also a viable formation mechanism for thick disks, and indeed high redshift disks are observed to be thick (Reshetnikov et al. 2003, Elmegreen & Elmegreen 2006b).

5. Conclusion

The UDF 6462 clump-cluster galaxy at $z = 1.57$ has a complex asymmetrical morphology, dominated by massive star-forming clumps. Spectroscopic observations of the $H\alpha$, [NII] and [SII] emission lines of this system using SINFONI on UT4 at ESO/VLT have revealed a velocity gradient throughout the system, possibly tracing global rotation with a circular velocity of about 100 km s^{-1} . A central peak in the velocity dispersion further suggests that this velocity gradient likely traces rotation. This is expected if this clump cluster formed by internal fragmentation of an unstable gas-rich primordial disk. The velocity field shows large irregularities and dispersions which would be an anomaly for classical spiral disks, but can be explained by interactions between clumps, as shown by our numerical model. The unstable-disk model presented here reproduces, under a chosen projection, both the main morphological and kinematical properties of UDF 6462.

An internal origin for clumpy disks is thus fully compatible with observed morphological and kinematical properties in the case of UDF 6462. This does not definitely rule out a merger origin for this clump cluster. Nevertheless, the rotation-like velocity field would not be necessarily expected this way, while it is predicted for internal instabilities in a gas-rich disks (BEE07). Furthermore, UDF 6462 shows signs of central enrichment in a bulge-like central condensation, and a global metallicity in agreement with the estimated disk mass. This also is consistent with internal clumpiness in a massive, gas-rich disk, and would be an unlikely coincidence for a merging system. A similar large-scale rotation-like velocity gradient is also found, although poorly resolved, in the nearby bent chain galaxy UDF 6911 at redshift $z = 2.07$.

Just like morphological asymmetries and clumpiness, large kinematical disturbances of several tens of km s^{-1} can be a natural consequence of the internal evolution of gas-rich primordial disks if they become unstable and fragment into large star-forming clumps once they have accreted enough mass. Spectroscopic data should be obtained on more clumpy galaxies, and a systematic comparison with model predictions should be performed, before general conclusions on the origin of chain and clump cluster galaxies can be obtained. At least, our present results show that even a severely disturbed case like UDF 6462 could actually be formed by internal evolution and that hierarchical mergers are not necessarily needed to explain the formation of such systems. Highly disturbed morphologies and/or disturbed kinematics with high velocity dispersions have often been attributed to mergers in the recent literature. We have here shown that such properties do not provide robust evidence for mergers, and may have an internal origin as well. Resolved spectroscopic data are needed to really constrain the origin of clumpy galaxies at high redshift on large samples, as well as large sets of numerical models to check that systematic kinematical classifications as in Flores et al. (2006) or Shapiro et al. (2008) can distinguish fragmented disks from merging systems.

If clumpy galaxies are formed by large instabilities in gas-rich primordial disks, as is likely the case for UDF 6462 and possibly also for UDF 6911, they can show large disturbances in their velocity field from one clump to the next one, but models presented here and in BEE07 predict that on the largest scales, velocity gradient tracing the initial ro-

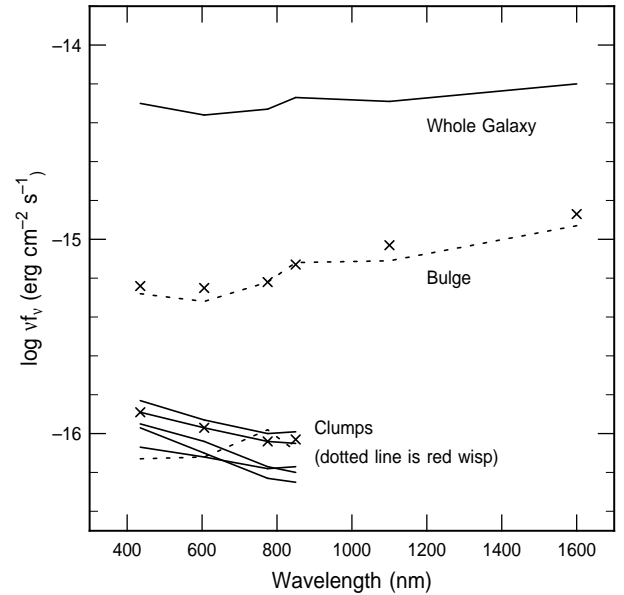


Fig. A.1. Spectral energy distributions of the whole system (top line), central bulge-like object (middle line), and several clumps (bottom left). Symbols are the best model fits for the bulge and for one of the clumps. A good fit is obtained for the clumps without an old stellar population, while the bulge has a ~ 1 Gyr old population. The 'red wisp' is a small and somewhat redder clump at ($\alpha=3h 32m 43.68s - \delta=-27^\circ 46' 58.8''$) close to the bulge itself. The typical uncertainties on the clump individual fluxes are 0.2 on $\log(\nu f_\nu)$ in the optical and 0.3-0.4 in the NIR, so that the difference between the central bulge and the other clumps is robust.

tation should be observed together with high velocity dispersions. High turbulent speeds observed in high-redshift disks (Genzel et al. 2006; Förster Schreiber et al. 2006) are in agreement with this scenario, as they increase the Jeans mass and enable the formation of large, massive clumps in gas-rich disks. Moreover, UV and optical star forming disks at high-redshift have high angular momentum compared to local disks (Bouché et al. 2007), which phases of clumpy evolution can contribute to dissipate rapidly while fueling bulges and shaping more concentrated disks with exponential profiles. The spectroscopic data presented in this paper thus support the hypothesis by Noguchi (1999), Immeli et al. (2004a,b), Elmegreen et al. (2005) and BEE07 that gas-rich primordial disks internally evolve through a clumpy phase into bright early-type disk galaxies with a massive exponential disk, a classical bulge, and possibly a central black hole.

Appendix A: Stellar population study of UDF 6462 bulge and star-forming clumps

The observed SEDs for the whole UDF 6462 galaxy, the bulge, and several clumps are shown in figure A.1, using NICMOS resolution for the bulge and ACS resolution for the clumps. The bulge is clearly redder than the clumps. The reddest clump is an extended region jutting off from the bulge and may be part of the bulge. Theoretical fits to the SED of one of the clumps and to the bulge SED (crosses) are shown; details of these models are in EE05. Extinction curves from Calzetti et al. (2000) and Leitherer et al. (2002) were used, and intergalactic absorption by Lyman lines was

included following Madau (1995). The basic population evolution models are from Bruzual & Charlot (2003) assuming a metallicity of 0.008, which is 0.4 solar, and a Chabrier (2003) IMF. Star formation is assumed to begin at some time prior to the redshift of the object and to decay exponentially with a characteristic time scale. The age of the region and the decay time, along with the extinction, are parameters of the fit. The best fits here require extinctions of $A_V = 0.6$ mag for the clump and $A_V = 1.2$ mag for the bulge. The models suggest that the central, reddish, bulge-like object has an age of around 1 Gyr (or even older if the actual extinction is the same as for the clumps), and the clumps have an age of ~ 50 Myr with a comparable decay time in the star formation rate. There appears to be no significant old stellar component in the clumps. If these clumps were separate galaxies in a merging process, they would have older stellar components in them and look redder. No other part is as red as the central bulge or the reddish wisp near it (see also Fig. 3), which further suggests that no clump is a separate galaxy. The bulge is bluer than bulges in moderate redshift galaxies (e.g., Zheng et al. 2004), which suggests some on-going star formation; however the relatively poor resolution of NICMOS compared to the bulge clump observed with the ACS allows younger structure to contaminate the bulge SED, which would bias the bulge color slightly towards the blue.

Appendix B: Metallicity distribution in galaxy mergers and fragmented disks

The models from BEE07 used to interpret the kinematics of UDF 6462 do not directly provide predictions on the gas metallicity. To support the interpretation of the observed metallicity distribution in Fig. 7 and Section 4.1, we show some Tree-SPH models including chemical evolution from Di Matteo et al. (2007), for clumpy star-forming systems formed by galaxy mergers and internal disk fragmentation.

B.1. Galaxy merger models

The galaxy merger models shown here are from Di Matteo et al. (2007) and the GALMER⁸ database (Chilingarian et al. in preparation). The merging disk galaxies start with a realistic radial metallicity gradient in their disk. These binary mergers often have two main star forming regions at the center of each galaxy, but massive star forming regions also form in at larger radii by instabilities in spiral arms or in tidal tails (see e.g., Elmegreen et al. 1993), sometimes giving a clump-cluster morphology in the gas distribution. The four cases shown in Fig. B.1 are early stage mergers that have been selected in the database for their clumpy morphology without any criterium related to the metallicity. They are representative of the majority of the ~ 900 models available in the database.

As shown in Fig. B.1, clump-cluster-like systems formed in early stages of galaxy mergers do not have a well organized metallicity gradient. In UDF 6462, the metals are observed to be centrally concentrated around the red protobulge and star formation takes place in the outer clumps. At the opposite, in these galaxy mergers models the star forming knots in the outer regions are associated to metallicity peaks. Even the outermost large star-forming regions in

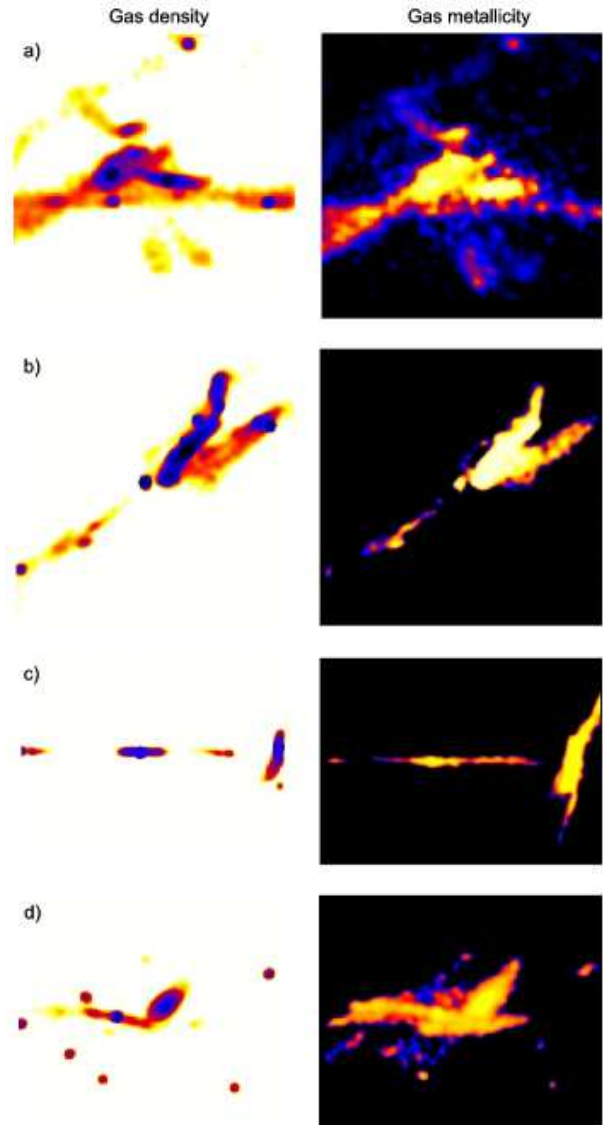


Fig. B.1. Gas density and metallicity maps in several galaxy merger models with a clumpy gas distribution. Outer star-forming regions can have been previously enriched in the inner disks of the progenitor spirals, like the tail to the bottom-left in case b, the clump to the left in case c, or the various external clumps in cases a and d. These cases are typical of the merger models from the GALMER database. Snapshots show between 25 and 40 kpc in radius and are all in log scale, with different intervals for each one as they represent different systems.

tidal tails around colliding galaxies, the TDG progenitors, are observationally known to have higher metallicities than classical disks outskirts, with quite often nearly-solar metallicities (e.g., Duc et al. 2000). Indeed, star-forming regions at large radii in mergers can have been previously enriched in inner regions and expelled by tidal forces. Hence, the radial metallicity gradient typical of disks is not preserved in the early phases of galaxy mergers (at least until the final relaxation) even when these have gas distribution similar to clumpy galaxies.

⁸ available at <http://galmer.obspm.fr>

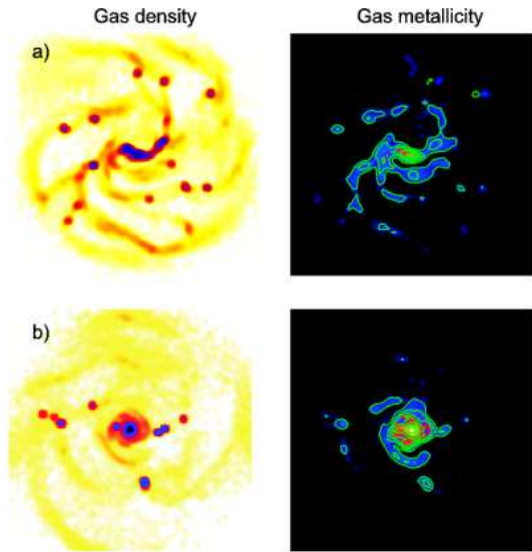


Fig. B.2. Clump-cluster model formed by internal disk fragmentation. The gas density and metallicity maps are shown at two stages in the evolution. Green contours on the metal maps are metallicity contours, linearly spaced from 0 to 0.05. Each box is 40×40 kpc. The star forming clumps have a moderate contribution to the metallicity distribution. The radial gradient from the progenitor disk is better preserved than in the merging of initially independent galaxies.

B.2. Disk fragmentation models

The model shown on Fig. B.2 is a gas-rich unstable disk, that gets fragmented in the same process as our dedicated model reproducing the kinematics of UDF 6462. Clumps form stars and contribute to the ISM enrichment, they interact and migrate inwards. Despite, a prominent metallicity peak remains clearly associated to the mass center, and no major metallicity peak is associated to the outer star forming clumps. The radial metallicity gradient typical of classical disks, and observed in UDF 6462, is hence best preserved if clump cluster galaxies form by the fragmentation of gas rich disks than in the merger of independent galaxies.

Acknowledgements. We thank the ESO Director General for allocating DDT time to this observing program. The numerical calculations were carried out on the vector computer NEC-SX8R of CEA/CCRT and supported by the Horizon project. Useful discussions with Nicolas Bouché, Pierre-Alain Duc, Françoise Combes and Chris Conselice are gratefully acknowledged. Suggestions by the referee and professional handling of the manuscript by the editor are appreciated.

References

Amram, P., Mendes de Oliveira, C., Plana, H., Balkowski, C., & Hernandez, O. 2007, *A&A*, 471, 753
 Angiras, R. A., Jog, C. J., Dwarakanath, K. S., & Verheijen, M. A. W. 2007, *MNRAS*, 378, 276
 Beckwith, S. V. W., Caldwell, J., Clampin, M., et al. 2003, in *Bulletin of the American Astronomical Society*, Vol. 35, 723
 Bonnet, H., Abuter, R., Baker, A., et al. 2004, *The Messenger*, 117, 17
 Bouché, N., Cresci, G., Davies, R., et al. 2007, *ApJ*, 671, 303
 Bournaud, F., Combes, F., Jog, C. J., & Puerari, I. 2005, *A&A*, 438, 507
 Bournaud, F., Elmegreen, B. G., & Elmegreen, D. M. 2007, *ApJ*, 670, 237
 Bournaud, F., Jog, C. J., & Combes, F. 2007, *A&A*, 476, 1179
 Bruzual, G., & Charlot, S. 2003, *MNRAS*, 344, 1000

Calzetti, D., Armus, L., Bohlin, R. C., Kinney, A. L., Koornneef, J., & Storchi-Bergmann, T. 2000, *ApJ*, 533, 682
 Carollo, C. M., Scarlata, C., Stiavelli, M., Wyse, R. F. G., & Mayer, L. 2007, *ApJ*, 658, 960
 Chabrier, G. 2003, *PASP*, 115, 763
 Chary, R. & Elbaz, D. 2001, *ApJ*, 556, 562
 Conselice, C. J. 2003, *ApJS*, 147, 1
 Conselice, C. J., Grogin, N. A., Jogee, S., et al. 2004, *ApJ*, 600, L139
 Conselice, C. J., Bundy, K., Ellis, R. S., Brichmann, J., Vogt, N. P., & Phillips, A. C. 2005, *ApJ*, 628, 160
 Conselice, C. J., Rajgor, S., & Myers, R. 2007, *MNRAS* submitted, astro-ph/0711.2333
 Cowie, L. L., Songaila, A., Hu, E. M., & Cohen, J. G. 1996, *AJ*, 112, 839
 Cox, T. J., Jonsson, P., Primack, J. R., & Somerville, R. S. 2006, *MNRAS*, 373, 1013
 Daddi, E., Cimatti, A., Renzini, A., et al. 2004, *ApJ*, 600, L127
 Daddi, E., Dannerbauer, H., Elbaz, D., et al. 2008, *ApJ*, 673, L21
 Daddi, E., Dickinson, M., Morrison, G., et al. 2007, *ApJ*, 670, 156
 Dalcanton, J. J. & Shectman, S. A. 1996, *ApJ*, 465, L9
 Di Matteo, P., Combes, F., Melchior, A.-L., & Semelin, B. 2007, *A&A*, 468, 61
 Dickinson, M. 2000, in *Philosophical Transactions of the Royal Society of London, Series A*, 358, 2001
 Donley, J. L., Koribalski, B. S., Staveley-Smith, L., et al. 2006, *MNRAS*, 369, 1741
 Duc, P.-A., Brinks, E., Springel, V., Pichardo, B., Weilbacher, P., & Mirabel, I. F. 2000, *AJ*, 120, 1238
 Eisenhauer, F., Abuter, R., Bickert, K., et al. 2003, in *Presented at the Society of Photo-Optical Instrumentation Engineers (SPIE) Conference*, Vol. 4841, M. Iye & A. F. M. Moorwood Editors, 1548–1561
 Elmegreen, B. G., Kaufman, M., & Thomasson, M. 1993, *ApJ*, 412, 90
 Elmegreen, B. G. & Elmegreen, D. M. 2005, *ApJ*, 627, 632
 Elmegreen, B. G., Elmegreen, D. M., Vollbach, D. R., Foster, E. R., & Ferguson, T. E. 2005, *ApJ*, 634, 101
 Elmegreen, D. M. 2007, in *IAU Symposium*, Vol. 235, ed. F. Combes & J. Palous, 376–380
 Elmegreen, D. M. & Elmegreen, B. G. 2006, *ApJ*, 651, 676
 Elmegreen, B. G. & Elmegreen, D. M. 2006b, *ApJ*, 650, 644
 Elmegreen, D. M., Elmegreen, B. G., Ferguson, T., & Mullan, B. 2007a, *ApJ*, 663, 734
 Elmegreen, D. M., Elmegreen, B. G., & Hirst, A. C. 2004, *ApJ*, 604, L21
 Elmegreen, D. M., Elmegreen, B. G., Ravindranath, S., & Coe, D. A. 2007b, *ApJ*, 658, 763
 Elmegreen, B. G., Bournaud, F., & Elmegreen, D. M. 2008b, *ApJ* submitted
 Erb, D. K., Shapley, A. E., Pettini, M., et al. 2006a, *ApJ*, 644, 813
 Erb, D. K., Steidel, C. C., Shapley, A. E., Pettini, M., Reddy, N. A., & Adelberger, K. L. 2006b, *ApJ*, 646, 107
 Flores, H., Hammer, F., Puech, M., Amram, P., & Balkowski, C. 2006, *A&A*, 455, 107
 Förster Schreiber, N. M., Genzel, R., Lehnert, M. D., et al. 2006, *ApJ*, 645, 1062
 Genzel, R., Tacconi, L. J., Eisenhauer, F., et al. 2006, *Nature*, 442, 786
 Giavalisco, M., Ferguson, H. C., Koekemoer, A. M., et al. 2004, *ApJ*, 600, L93
 Gillessen, S., Davies, R., Kissler-Patig, M., et al. 2005, *The Messenger*, 120, 26
 Goldader, J. D., Meurer, G., Heckman, T. M., Seibert, M., Sanders, D. B., Calzetti, D., & Steidel, C. C. 2002, *ApJ*, 568, 651
 Halliday, C., Daddi, E., Cimatti, A. et al. 2008, *A&A*, 479, 417
 Immeli, A., Samland, M., Gerhard, O., & Westera, P. 2004a, *A&A*, 413, 547
 Immeli, A., Samland, M., Westera, P., & Gerhard, O. 2004b, *ApJ*, 611, 20
 Jogee, S., Miller, S., Penner, K., et al. 2008, astro-ph/0802.3901
 Johansson, P. H., Naab, T., & Burkert, A. 2008, *ApJ* submitted, astro-ph/0802.0210
 Kennicutt, R. C., Jr. 1998a, *ARA&A*, 36, 189
 Kennicutt, Jr., R. C. 1998b, *ApJ*, 498, 541
 Lehnert, M. D., & Heckman, T. M. 1996, *ApJ*, 462, 651
 Leitherer, C., Li, I.-H., Calzetti, D., & Heckman, T. M. 2002, *ApJS*, 140, 303

- Liang, Y. C., Hammer, F., Flores, H., Elbaz, D., Marcillac, D., & Cesarsky, C. J. 2004, *A&A*, 423, 867
- Madau, P. 1995, *ApJ*, 441, 18
- Modigliani, A., Hummel, W., Abuter, R., et al. 2007, *ArXiv astro-ph/0701297*
- Moran, E. C., Lehnert, M. D., & Helfand, D. J. 1999, *ApJ*, 526, 649
- Moustakas, L. A., Casertano, S., Conselice, C. J., et al. 2004, *ApJ*, 600, L131
- Nesvadba, N. P. H., Lehnert, M. D., Eisenhauer, F. et al. 2006, *ApJ*, 650, 661
- Noguchi, M. 1999, *ApJ*, 514, 77
- O’Neil, K., Bothun, G. D., & Impey, C. D. 2000, *ApJS*, 128, 99
- Pettini, M. & Pagel, B. E. J. 2004, *MNRAS*, 348, L59
- Pohlen, M., Erwin, P., Trujillo, I., & Beckman, J. E. 2007, *ArXiv:astro-ph/0706.3830*, 706
- Puech, M., Hammer, F., Flores, H., Östlin, G., & Marquart, T. 2006, *A&A*, 455, 119
- Reichard, T. A., Heckman, T. M., Rudnick, G., Brinchmann, J., & Kauffmann, G. 2007, *ApJ* in press, *astro-ph/0710.0589*
- Rots, A. H. 1975, *A&A*, 45, 43
- Shapiro, K. L., Genzel, R., Förster Schreiber, N. M., et al. 2008, *ApJ* in press (*astro-ph/0802.0879*)
- Smith, A. M., Collins, N. R., Waller, W. H., et al. 2001, *ApJ*, 546, 829
- Storchi-Bergmann, T., Calzetti, D., & Kinney, A. L. 1994, *ApJ*, 429, 572
- Taniguchi, Y. & Shioya, Y. 2001, *ApJ*, 547, 146
- Tody, D. 1993 in *ASP Conference Series Vol. 52*, R. J. Hanisch, R. J. V. Brissenden & J. Barnes Ed., 173
- Tremonti, C. A., Heckman, T. M., Kauffmann, G., et al. 2004, *ApJ*, 613, 898
- Trujillo, I., Förster Schreiber, N. M., Rudnick, G., et al. 2006, *ApJ*, 650, 18
- van den Bergh, S., Abraham, R. G., Ellis, R. S., et al. 1996, *AJ*, 112, 359
- Vanzella, E., Cristiani, S., Dickinson, M., et al. 2006, *A&A*, 454, 423
- Vanzella, E., Cristiani, S., Dickinson, M., et al. 2008, *A&A*, 478, 83
- Weiner, B. J., Willmer, C. N. A., Faber, S. M., et al. 2006, *ApJ*, 653, 1049
- Yoachim, P., & Dalcanton, J. J. 2005, *ApJ*, 624, 701
- Yoachim, P., & Dalcanton, J. J. 2006, *AJ*, 131, 226
- Zheng, X. Z., Hammer, F., Flores, H., Assémat, F., & Pelat, D. 2004, *A&A*, 421, 847